ADVANCES IN APPLIED CERAMICS
2020, VOL. 119, NOS. 5–6, 364–371
https://doi.org/10.1080/17436753.2019.1625567

β-Tricalcium phosphate-silica aerogel as an alternative bioactive ceramic for the potential use in dentistry

Viktória Hegedűs[a], Farkas Kerényi [b], Róbert Boda[c], Dóra Horváth[c], István Lázár [d], Enikő Tóth-Győri[d], Balázs Dezső[e] and Csaba Hegedus[f]

[a]Department of Pediatric Dentistry and Orthodontics Faculty of Dentistry, University of Debrecen, Debrecen, Hungary; [b]Department of Biomaterials and Prosthetic Dentistry Faculty of Dentistry, University of Debrecen, Debrecen, Hungary; [c]Department of Oral and Maxillofacial Surgery Faculty of Dentistry, University of Debrecen, Debrecen, Hungary; [d]Department of Inorganic and Analytical Chemistry Faculty of Science, University of Debrecen, Debrecen, Hungary; [e]Department of Oral Pathology and Microbiology Faculty of Dentistry, University of Debrecen, Debrecen, Hungary; [f]Department of Biomaterials and Prosthetic Dentistry Faculty of Dentistry, University of Debrecen, Debrecen, Hungary

ABSTRACT

In this study, a mesoporous silica-aerogel with β-tricalcium phosphate (β-TCP-AE) was manufactured. The effect of β-TCP-AE on gene expressions (BMP2, BMP7, Runx2 and OSX) of SAOS-2 cells was tested. For the in vivo evaluation, the 'calvaria critical-size defect' model was used: following one and three months of the artificial surgical bone defects filled with β-TCP-AE, histopathological analyses were performed. Gene expression studies demonstrated a mild osteoblastic differentiation of the SAOS-2 cells triggered after seven days of β-TCP-AE-treatment. Digital histology of rat's calvarial bone defects reconstructed with β-TCP-AE showed that after one month, calcifications and early ossifications developed with the presence of capillary-rich fibrose inflammation and remnants of exogenous compounds which nearly dissappeared by the third month, and replaced with multiple newly formed bone islets mediated by osteoblasts. Based on our results this bioceramic compound appears to have favourable properties for the use as a scaffold in the reconstructive medical practice.

ARTICLE HISTORY
Received 12 November 2017
Revised 27 February 2019
Accepted 11 March 2019

KEYWORDS
β-tricalcium-phosphate; bioactive ceramic; silica-aerogel; scaffold; SAOS-2; ossification; bone defect; osteoblast; histo-morphology

Introduction

Nowadays progressively growing parts of the reconstructive medicine incorporate different artificial materials which facilitate the healing or remodelling of the human tissues at sites of defects. One of these special materials are the bioceramics, like glass ceramics or bioglasses, which appear useful both in the general medical practice and dentistry procedures or applications owing to the specially designed nature [1].

Since the first bioglass, introduced by L. L. Hench in 1969, variously improved types of glasses and ceramics have been developed [2].

Such defects where large bone replacements are indispensable including coarse fractures, cysts (e.g. aneurysmal bone cyst) or following a surgical removal of extensively infiltrating tumour lesions, there is a need for a bony substitution which can be autograft, allograft (of human bone), xenograft (e.g. bovine or porcine derived bones) or the use of alloplast from various external sources (polycrystalline ceramic form of pure densely sintered hydroxyapatite, coralline porous non-resorbable hydroxyapatite, resorbable nonceramic hydroxyapatite, β-tricalcium phosphate (β-TCP), biphasic alloplastic materials, calcium phosphate cements, bioactive glasses, biocompatible osteoinductive polymers, ceramics and bioactive molecules). For the healing of a bone defect both the natural bone grafts and the tissue-inducing engineered inorganic replacement-parts need to have good oxygen and nutrients supplies for a long-term solidified-anchoring integration of the inserted material with the recipient's tissue components [3]. Therefore, the tissue-defect and the consecutive inflammation-induced vasculogenesis including with the mobilisation/activation of newly formed accessory mesenchymal cells appear the major initial indispensable event for a successful tissue-defect's substitution and/or remodelling. In this respect, cellular and structural requirements need to be present for the new bone formation including stem cells, marrow-stromal cells, osteoblasts, chondrocytes and fibroblasts, and scaffolding provided by the grafted material which may be autograft, allograft, xenograft or alloplast; the latter should exhibit the following structural properties: appropriate porosity, pore size, pore interconnection, good mechanical scaffolding properties, and the biological characteristics with osteoconductive, osteoinductive (or both) features to mobilise the recipient's tissue-derived signalling molecules including cytokines, growth factors and pro-

CONTACT Csaba Hegedus hegedus.csaba.prof@dental.unideb.hu

inflammatory factors and molecules involved in cell activation, migration, adhesion, and cell–cell communication.

The aim of this study is to prepare and characterise mesoporous silica-based aerogels (AE) containing β-tricalcium phosphate (β-TCP-AE) as bioactive agents for potential dental applications. Based on the in vivo experiments on rat calvarial bone's defect, the β-TCP-AE compound exhibits appropriate scaffolding and in turn induces multifocal ossification to fill the entire lesion to integrate and anchor to the recipient tissue within three months.

Material and methods

Preparation of silica aerogel-based composites

The samples containing β-TCP were prepared by the base-catalysed sol–gel technique [4]. The following general recipe was applied: first, two solutions ('A' and 'B') were prepared. Solution 'A' was made of 45.0 mL (1.112 mol) methanol, 8.00 mL (0.444 mol) distilled water, 15.00 mL (0.113 mol) diluted (1:1) NH_3 solution (obtained by diluting 10.0 mL of 25% NH_3 solution with 10.0 mL water) and 30.0 mL (0.100 mol) urea solution (obtained by dissolving 10.0 g urea in 50.0 mL methanol). Solution 'B' contained 35.0 mL (0.865 mol) methanol and 15.0 mL (0.102 mol) tetramethoxysilane. 5.00 g (0.0161 mol) β-TCP and 5.00 g cellulose were added to solution 'A' under intensive stirring. Solution 'A' and 'B' were then mixed under vigorous stirring.

In order to avoid aggregation of the additives, the sol was stirred until it turned very viscous, but gel formation had not yet began. At that point, it was transferred into cylindrical plastic moulds (66 × 28 mm), then sealed with parafilm and allowed to gel at room temperature overnight.

After changing the solvent from methanol to acetone in several steps, the gels were stored in a copious volume (2 L) of freshly distilled dry acetone for three days. The supercritical drying was carried out in a custom-made high-pressure reactor according to a general procedure published in previous works [5–7].

Aerogel composite monoliths were calcined in a programmable temperature furnace in order to achieve suitable mechanical strength. In the first step, the disposable porogen cellulose and adsorbed organic molecules were burned out at 500°C/8 h. Heat treatment of the specimens was continued by elevating the temperature in 100°C increments. Each target temperature was reached in 3 h and kept constant for 1 h, followed by a spontaneous cool-down to room temperature. After that, the dimensions and weights were recorded and density values calculated. Averaged density values and standard deviations were calculated from the data points recorded for six samples.

Characterisation

Nitrogen gas adsorption/desorption porosimetry measurements were performed on a Quantachrome Nova 2200e surface area and porosity analyser (Quantachrome Instruments, Boynton Beach, FL, USA). The calcined pieces of samples were grinded in a mortar and outgassed under vacuum at 300°C for 3 h before the measurements.

Scanning electron micrographs (SEMs) were recorded on a Hitachi S-4300 instrument (Hitachi Ltd., Tokyo, Japan) equipped with a Bruker energy dispersive X-ray spectrometer (Bruker Corporation, Billerica, MA, USA). The surfaces were covered by a sputtered gold conductive layer, and the samples were surrounded by a layer of Wood's metal to increase electric charge dissipation. A 5 kV accelerating voltage was used for taking high-resolution pictures.

Cell culture

SAOS-2 cells were cultured in Dulbecco's Modified Eagle's Medium (DMEM, low glucose; Sigma, USA) supplemented with 10% foetal bovine serum, 1% antibiotic-antimycotic solution and 1% Glutamax (all from Gibco, USA) in a humidified incubator at 37°C and 5% CO2. After reaching confluence, cells were trypsinised and 2×104 cells/cm^2 were seeded into 24-well-plates (Nunc, Denmark). Following adherence, the culture medium (CM) was changed with CM containing either 0.2 mg/ml grinded AE or 0.2 mg/ml grinded β-TCP-AE (Figure 6(A)). The AE and β-TCP-AE particles then sunk onto the cells to achieve direct contact between the material particles and the cells. The medium was then changed every second day. All samples were taken on the seventh day for examinations.

Viability and cytotoxicity assay

The viability of the cells and the cytotoxicity of the materials were examined using alamarBlue Cell Viability Reagent (Invitrogen, USA) assay according to the manufacturer's instructions. Shortly, 1 ml of the alamarBlue diluted to 10x in CM was placed on each sample. After 2 h of incubation at 37°C, the fluorescence of 200 µl solution from each sample was measured (exc. 544 nm, em. 595 nm) in a Hidex Sense microplate reader (Hidex, Finland).

Alkaline phosphatase (ALP) activity assay

After washing in PBS, cells were lysed in lysis buffer (10 mM Tris-HCl pH7.4, 100 mM NaCl, 1 mM EDTA, 1% Triton X-100, 1% PIC, 1% PMSF). Then the cell debris were removed from the lysed samples with centrifugation at 10,000 g for 10 min at 4°C in a Centrifuge 5810 R (Eppendorf, Germany). Supernatant

was transferred to another microcentrifuge tube and used to determine the alkaline phosphatase activity by mixing the cell lysates with the enzyme substrate p-nitrophenyl phosphate (Sigma-Aldrich, USA). The absorbance of the samples was measured at 405 nm in a Hidex Sense microplate reader (Hidex, Finland). ALP activity was normalised to protein concentration determined using BCA Protein Assay kit (Pierce, USA).

Gene expression analysis by qRT-PCR

Total RNA was extracted with Quick RNA MiniPrep kit (Zymo Research, USA) according to the manufacturer's instructions. From each sample, 1000 ng RNA was used for the reverse transcription with High Capacity cDNA Reverse Transcription Kit (Applied Biosystems, USA). The qPCR was performed using HOT FIREPol Probe qPCR Mix Plus (no ROX) (Solis Biodyne, Estonia) enzyme and gene-specific TaqMan probes (Applied Biosystems, USA) (see Table 1) in a LightCycler 480 instrument (Roche, Switzerland). GAPDH was used as an internal reference gene for all measurements. Gene expression levels were calculated based on the ΔCp method.

In vivo study

For the in vivo experiments, osteointegration was investigated in association with the inserted AE or β-TCP-AE samples in rat's 'calvaria critical size defect model'. Animal surgeries were performed under the authorisation of University of Debrecen Institutional Animal Care and Use Comitee (7/15/DEMÁB). Nineteen adult male Wistar rats weighing 250–300 g were used in this study kept on standard diet with water ad libitum. Animals were anesthetised by intraperitoneal injection of ketamine (CP-Ketamin 10%, Produlab Pharma B.V., Raamsdonksveer, Holland) and xylazine (Xylazin 2%, CP-Pharma, Burgdorf, Germany) in 2:1 ratio (0.5–0.55 ml/animal). A sagittal skin incision was performed on the skull with a matching incision on the periosteum. An 8 mm diameter full-thickness defect was created in the midline of the parietal bone region with a trephine-bur under saline irrigation. The bone was then removed with a care to avoid dura injury.

The bone defect in group I was left empty for control; in group II, a granulate of the AE material was used ($n = 6$); in group III, β-TCP-AE composite granulates were implanted to fill the site of the bone defect ($n = 6$).

The periosteum and the skin were than closed in two layers with resorbable sutures. Animals were terminated at 1 and 3 months after surgery ($n = 3$ for either the 1-month or the 3-month groups). Transcardial saline perfusion was applied to reduce the presence of blood in the specimen. Skull was then harvested together with the periosteum and the dura mater for histopathology.

Table 1. List of TaqMan probes used for qPCR to examine osteoblastic differentiation of SAOS-2 cells in vitro.

Gene	Abbreviation	TaqMan ID
Bone morphogenic protein 2	BMP-2	Hs00154192_m1
Bone morphogenic protein 7	BMP-7	Hs00233476_m1
Runt-related transcription factor 2	Runx2	Hs00231692_m1
Osterix	OSX	Hs00541729_m1
Glyceraldehyde 3-phosphate dehydrogenase	GAPDH	Hs02758991_g1

Preparing tissue sections for histopathology

Bone tissue samples (n = 3 for either the 1-month or the 3-month groups) exhibiting the cylindrical calvarial bone defect filled with AE or β-TCP-AE compound or left unfilled (control) were fixed in 10% of buffered formaldehyde (pH 7.4) followed by decalcification in 4% EDTA and the staining with hematoxylin–eosin (HE) and van Gieson were carried out on deparaffinised sections with standard methods as described earlier [8]. Peroxidase-based immunohistochemical reactions were also made on antigen-retrieved sections as described previously [9] using rabbit monoclonal primary antibodies to Ki-67 (Abcam, UK) followed by peroxidase-labelled anti-rabbit immunoglobulin treatment which was then developed with VIP-chromogen (Vector Labs, UK). The stained sections were then digitalised using Panoramic MIDI digital slide scanner (3D-Histech-Zeiss, Budapest, Hungary) equipped with Hitachi (HV-F22CL) 3CCD progressive scan colour camera. Image analysis was performed by the HistoQuant application of Panoramic viewer software 1.15.2 (3D-Histotech) as described in detail earlier [10].

Statistical analysis

Data are reported as mean ± standard deviation (SD) from at least three separate experiments. One-way ANOVA was used to analyse the differences between treatment groups. A statistically significant difference was reported if $p = 0.05$ or less.

Results and discussion

Characterisation and porositystudy of the samples

The porosity of the silica aerogel matrix material was determined by nitrogen adsorption/desorption porosimetry. The obtained isotherm (Figure 1) can be classified as type IV, which is typical of mesoporous silica materials. The samples exhibit the presence of both macropores and mesopores (indicated by the sharply increasing adsorption isotherm above $P/P_0 = 0.9$ and the presence of the hysteresis loop). The pore size distribution curve (Figure 2) was calculated by the Barrett–

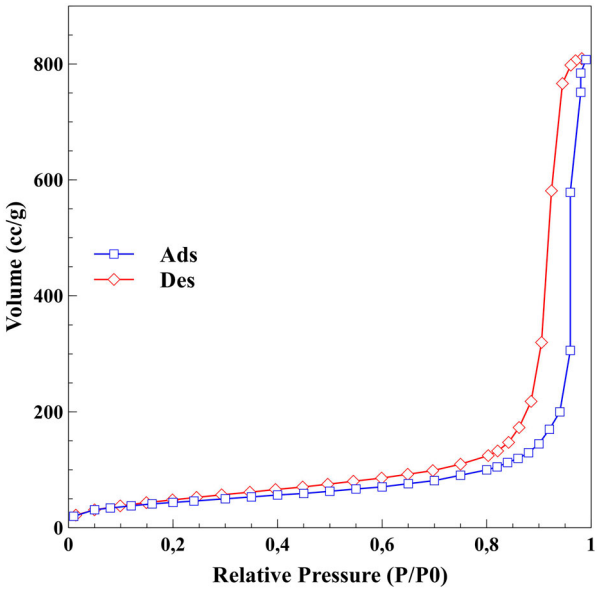

Figure 1. Adsorption (Ads) and desorption (Des) isotherms of the aerogel-based composite material. Hysteresis loop and shape of the curves indicate the presence of both macro- and mesopores.

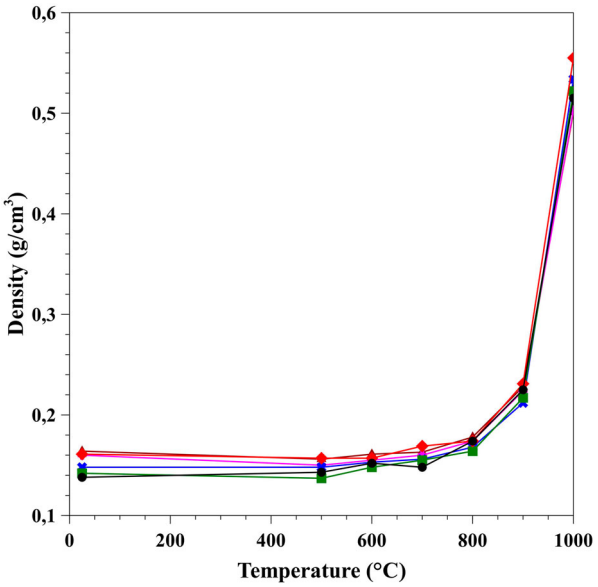

Figure 3. Change of densities of the samples as a function of heating temperature. The initial 0.15 g/cm^3 increased up to 0.52 g/cm^3 after the final heating step, and resulted in an increased mechanical strength.

Joyner–Halenda (BJH) method for the desorption branch. The main feature of the curve is that the pore size distribution is unimodal, and the dominant pore size is at around 25 nm. The calculated Brunauer–Emmett–Teller surface area was 160.4 m^2/g, which is very high compared to other artificial bone substitute materials. Larger than 200 nm pores present in the samples cannot be characterised by nitrogen adsorption–desorption porosimetry, due to the limitations of the method. Therefore, dark field optical microscopy and scanning electron microscopy (SEM) were used to show the distribution of guest particles, as well as for the characterisation of the micrometre-range pores in the tested materials, respectively (Figures 4 and 5).

The densities of the samples were calculated after the supercritical drying and each heating sections. The obtained values are shown in Figure 3. At room temperature, the density was 0.15 ± 0.01 g/cm^3 and it virtually has not changed on heating at 500°C. The

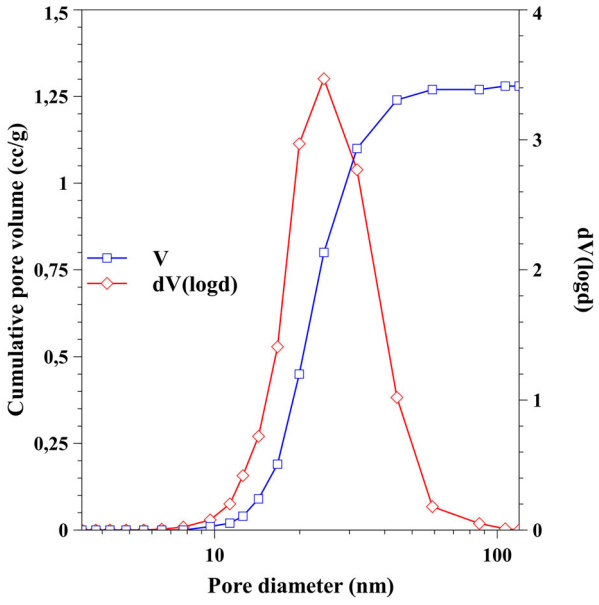

Figure 2. Pore size distribution curve (◇) and cumulative pore volume (□) of the samples calculated from desorption branch of the isotherm by the BJH method.

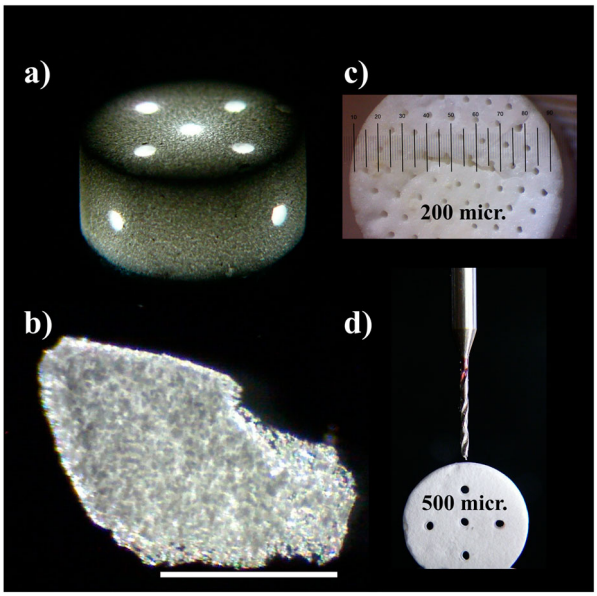

Figure 4. Optical microscopy images of sintered β-TCP-AE composites. (a) mould-casted monolitic sample with diagonally drilled through-channels of 500 µm diameter, (b) dark field image of a chip shattered from a monolit shows transparent silica aerogel matrix and opalescent granules of the embedded tricalcium phosphate plus the high-porosity regions. Scalebar is 1 mm, (c) mould-templated monolitic cylindrical sample with longitudinally arranged set of 200 µm diameter channels, (d) demonstration of the drilling process.

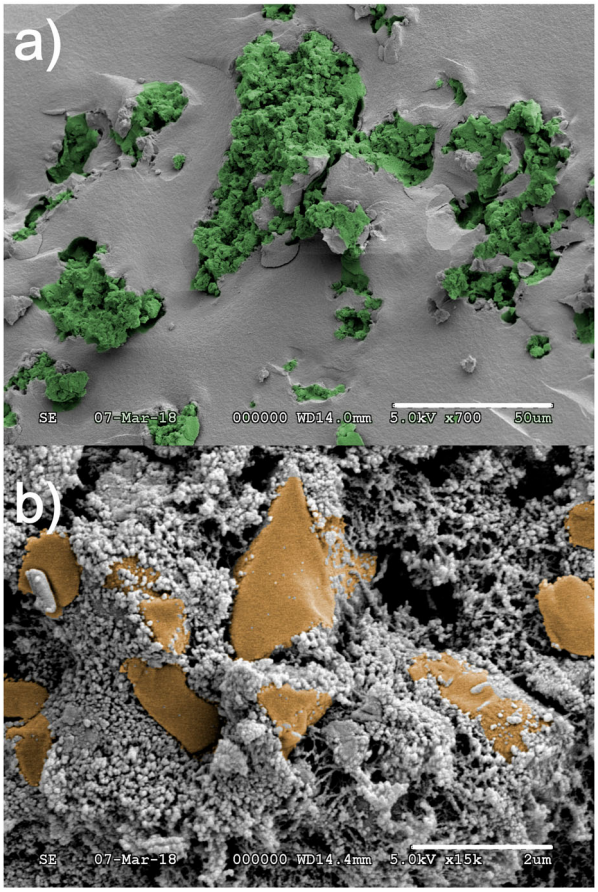

Figure 5. Scanning electron microscopy (SEM) images of fresh fracture surfaces of a β-TCP-aerogel composite (β-TCP-AE) in 700 x and 15k x magnification. (a) Uneven surface indicates highly porous, TCP containing regions. Pore diameters may go up to 20 μm. Smoother surface shows the porous silica aerogel matrix of 25 nm pore size. (b) Magnified view of a TCP-containing region. The bigger particles show tricalcium phosphate crystals embedded in silica aerogel matrix. Coral-like silica tissues are left behind after burning out microcrystalline cellulose from the matrix.

explanation is that, loss of weight due to burning-out cellulose was compensated by the shrinking of the specimens, and resulted in a seemingly unchanged density value. In between 500°C to 900°C weight loss of the samples are less pronounced and is associated with the removal of all adsorbed and loss of some structural water. The latter one is the result of the increasing condensation of neighbouring silanol groups. Between 900°C and 1000°C the density increased very sharply, as the endothermic water loss became the dominant process, and was associated with the viscous flow of the silica matrix, which also decreased of the specific surface area. The final density was 0.52 ± 0.02 g/cm^3.

After reaching the final density and mechanical strength, the silica aerogel-based β-TCP composite proved to be a very versatile and universally adaptable material. It is widely known, that for the new bone formation and tissue ingrowth, approximately 300 micrometer-sized pores are required. We have demonstrated that the sol–gel technology, combined either with templated moulding (Figure 4(c)), or a milling process (Figure 4(d)) can be equally used for shaping specimens and to provide the necessary large pores in any size and geometrical arrangement. Optical microscopy picture of a machined monolit (Figure 4 (a)) and its fragmented chip (Figure 4(c)) in lower (5x) and higher (50x) magnification shows granular distribution of β-TCP in the transparent silica aerogel matrix.

SEM study of a fresh fracture surface of β-TCP-AE revealed that, after burning out the disposable porogen cellulose, sponge-like or coral-like regions were formed (Figure 5(a)), in which the pore sizes are in the 1–20 μm range. This provides a good accessibility of the β-TCP particles both in simulated body fluid (SBF) and *in vivo* (Figure 5(b)).

A unique advantage of β-TCP-AEis that, unlike traditional synthetic bone substitutes, the aerogel matrix material has an entirely open pore structure. It ispermeable for smaller molecules like dissolved oxygen and nutrients, and provides a vivid environment for cell growth. Although the active component of the β-TCP-AE composite is β-TCP, the silica part also takes an important role. It is known, that water soluble silicates play an important role in the type I collagen formation [11]. The solubility of silica aerogel is much higher, than that of the crystalline silica. Application of this new material in living tissues may provide sufficient concentration of silicate to help collagen production and thus, to boostbone regeneration.

Viability of SAOS-2 cells

To examine whether the aerogel or the aerogel composite is cytotoxic for the SAOS-2 cells, a viability and proliferation assay was conducted using alamarBlue Cell Viability Reagent. After one week culture of SAOS-2 cells with aerogel, the alamarBlue assay shows no significant difference in proliferation compared to the control grown in CM only. Cultured with the composite β-TCP-AE, there is a slight but significant decrease in proliferation compared either to the control or to the cells cultured with AE (Figure 6(B)).

While SAOS-2 cells are differentiating to osteoblasts, cells are dying mainly through programmed cell death process of apoptosis but a notable part of the cells are dying because of necrosis [12]. It has been shown that bioceramics also can decrease the proliferation of the SAOS-2 cells [13]. Moreover, in the literature, we cannot find any sign of cytotoxic effect of β-TCP. So we concluded that this slight decrease in proliferation of SAOS-2 cells cultured with β-TCP-AE is rather indicates the process of osteogenic differentiation than the cytotoxicity of the material.

Alkaline phosphatase activity

While these materials are not toxic for the cells, their ability to induce osteoblastic differentiation of SAOS-

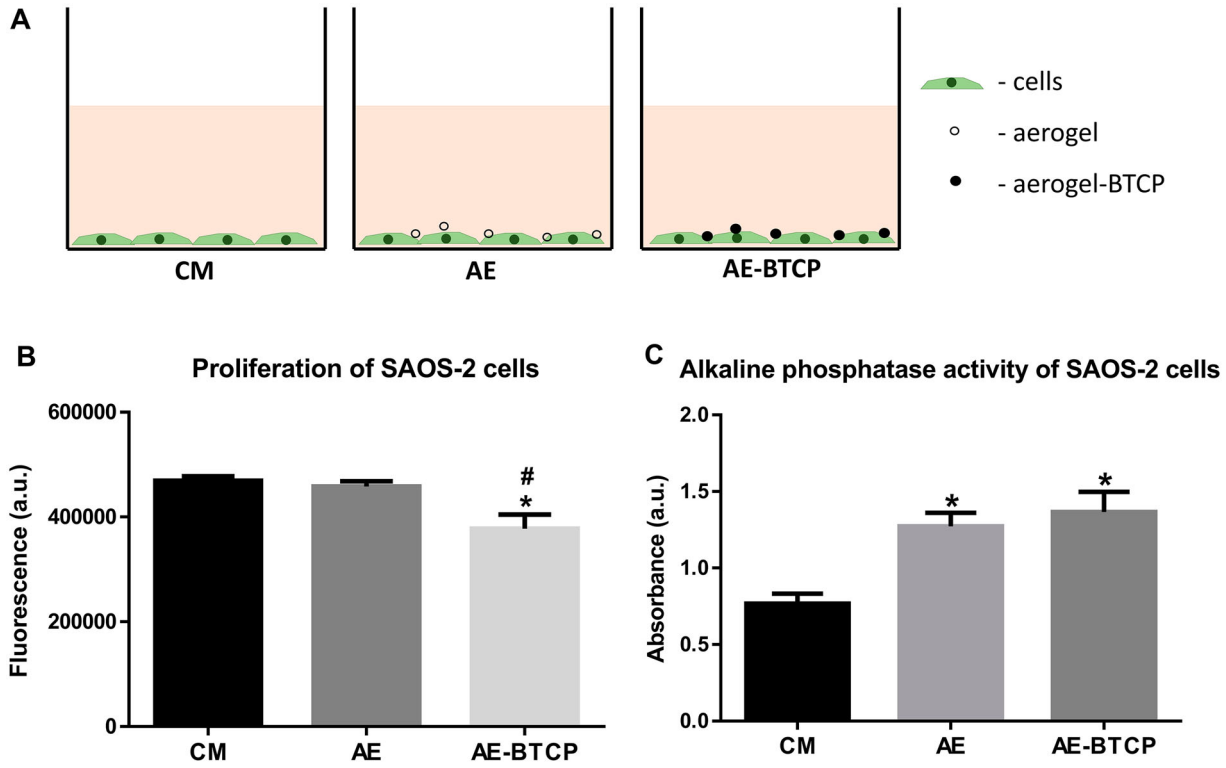

Figure 6. The design of the experiment – SAOS-2 cells were cultured in culture medium alone (CM) or in culture medium either with aerogel (AE) or β-TCP-aerogel composite (β-TCP-AE) granules for seven days (A). Proliferation of SAOS-2 cells after seven days examined with alamarBlue assay (B). Alkaline phosphatase activity of SAOS-2 cells measured after seven days (C). * – significant difference compared to CM ($p \leq 0.05$); # – significant difference between AE and B-TCP-AE ($p \leq 0.05$).

2 cells was examined. First, an alkaline phosphatase activity test (ALP-test) was carried out. The ALP-test shows a mild but significant increase in the samples cultured either with AE or with β-TCP-AE but there is no difference between the AE and the β-TCP-AE samples. While the increase of the alkaline phosphatase activity is a marker of the osteoblastic differentiation, this result supports our previous assumption that the SAOS-2 cells started differentiating.

Gene expression analysis

The expression of several genes involved in osteoblastic differentiation (BMP-2, Runx2, BMP-7 and osterix) was also examined. After one week culture of SAOS-2 cells, the gene expression in cells cultured with aerogel shows no significant difference compared to the control (CM) at least in case of the examined genes (Figure 7). There is a somewhat but not significantly higher BMP-7 and BMP-2 expression in β-TCP-AE compared either to the CM or to the AE samples (Figure 7(A, B)). However, the cells cultured with β-TCP-AE show significantly higher Runx2 expression compared to the CM but there is no significant difference in β-TCP-AE compared to AE (Figure 7(C)). The expression of OSX did not change at all after seven days (Figure 7(D)).

During osteoblastic differentiation, Runx2 is the master transcription factor that orchestrates either directly or indirectly the expression of other genes involved in the osteoblastic differentiation. Osterix (OSX) is also a very important transcription factor but it acts downstream of Runx2. The level of BMPs looks elevating but not significantly on the seventh day. So we proposed that the expression of OSX and BMPs would be significantly increased later in these settings of experiment. However, the increased Runx2 expression clearly shows the osteoblastic differentiation of SAOS-2 cells.

Taken together our *in vitro* results, it can be stated that, under the influence of the scaffold material, the SAOS-2 cells have already started to differentiate to osteoblasts at the seventh day.

Histological analysis

Based on image analyses on digitally scanned tissue sections, after 1 month of bone defect treatments with β-TCP-AE (group III) dense sub-acute inflammation developed with capillary-rich granulation tissue formation with fibrosis and scarring that showed multifocal calcifications and early bone formations in association with the presence of β-TCP-AE granular deposits (Figure 8(A, B)). According to the morphological analysis, the inflammatory infiltrates were mainly composed of PMNs (polymorphonuclear leukocytes) and macrophages with the presence of fibroblasts, all in active cell cycle (Figure 8(C)), the latter cells producing collagenous extracellular matrix.

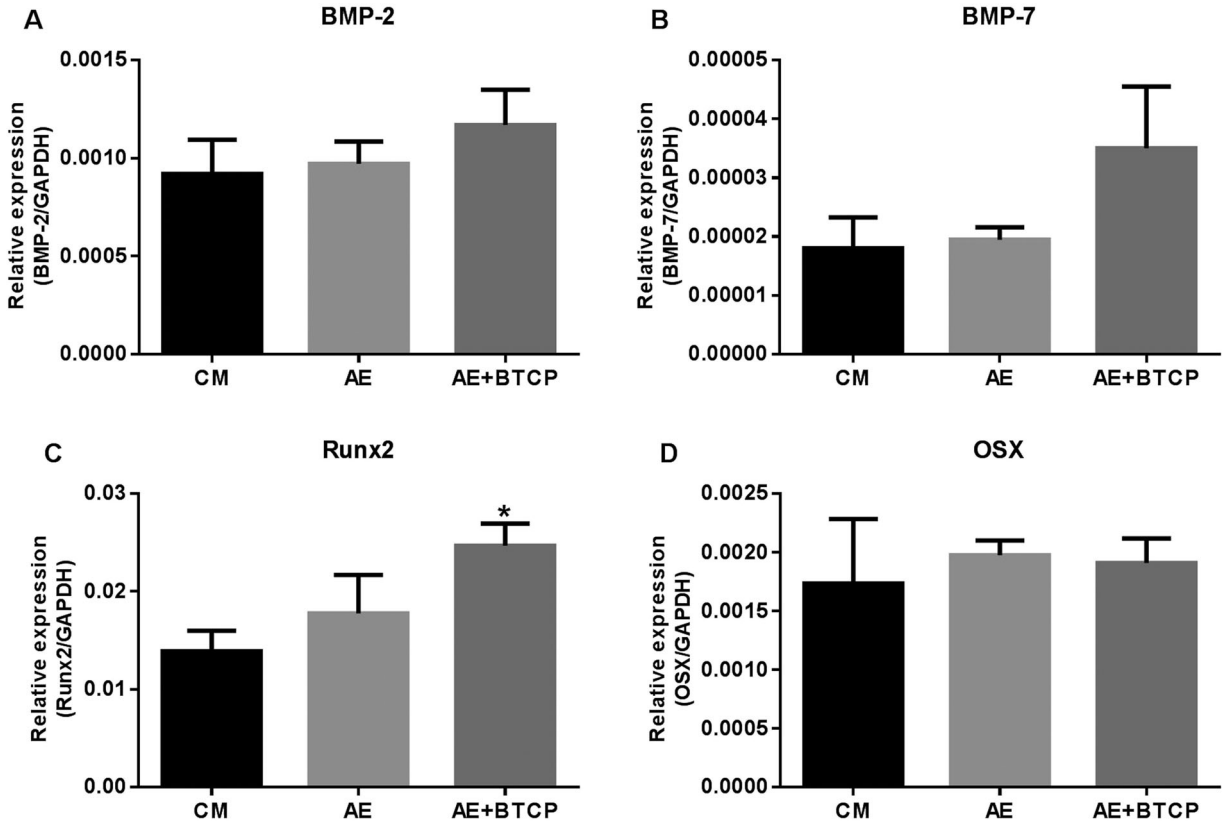

Figure 7. Gene expression analysis of SAOS-2 cells after seven days. The graphs show relative expression. Each gene was normalised to GAPDH. BMP-2 (A) and BMP-7 (B) show somewhat but not significant increase in the B-TCP-AE sample compared to the control (CM) or to the AE samples. Runx2 shows a slight but not significant increase in the AE sample and a significant increase in the B-TCP-AE sample compared to the CM. (C). There is no significant difference in OSX expression neither in the AE nor the β-TCP-AE samples compared to CM (D). * – significant difference compared to CM ($p \leq 0.05$).

Three months later of β-TCP-AE insertion into the bone defect, most of the β-TCP-AE compounds became eliminated and the number of inflammatory cells decreased significantly while solid and compact bone islets developed that were embedded into less cellular connective tissue indicating that an intense ossification is in progress (Figure 8(D)). At this stage of remodelling, newly formed bone-associated osteoblasts increased in number (Figure 8(E)), and mainly these cells are those which show active cell cycle confirmed by the Ki-67 nuclear immunolabelling (Figure 8(F)). As opposed, the bone defect specimens that were substituted with no material (control, group I) exhibited fibrosed inflammatory tissue replacement with moderate degree of ossification mainly along the internal rim of the bone defect, only; however, AE-treatment (group II) resulted in a similar but less intense ossification compared to the β-TCP-AE groups, predominantly detected at 3 months of bone injuries (not shown).

Conclusion

In our study, a silica-aerogel-based composite with β-TCP was manufactured which proved to be not toxic on cell lines applied. According to the results of the in vitro studies, the β-TCP containing silica-based aerogels can trigger mild osteoblastic differentiation of even on undifferentiated SAOS-2 osteosarcoma cells after one week of treatment. Most importantly, the in vivo study demonstrated that following β-TCP-AE insertion into the bone defect of the rats' calvarial bones, there is an intense injury- and exogenous material-associated consecutive inflammation with capillary-rich granulation tissue formation leading to fibrosis and early dystrophic calcifications which in turn induce incipient ossification, probably triggered by the β-TCP, that can be detected at the first month of reconstructive surgery. It is likely that these activated cellular components together with the presence of excess amounts of calcium from β-TCP and the scaffolding support component provided by the silica aerogel all drive the cells further stimulations toward to osteoblastic activations resulting in new bone formations at multifocal sites which could be demonstrated at the third month of β-TCP-AE compound's implantation. Based on the histopathology, the newly formed ossifying tissues appear keep growing on to replace the fibros tissues and to integrate and anchor to the host's bone avidly resulting in a solid plug – a sign of remodelling. In concert with this explanation, the tissue specimens obtained from the three months group showed well developed multiple solid bone tissues an associated high number of osteoblasts in active cell cycle and decreasing number of inflammatory cells

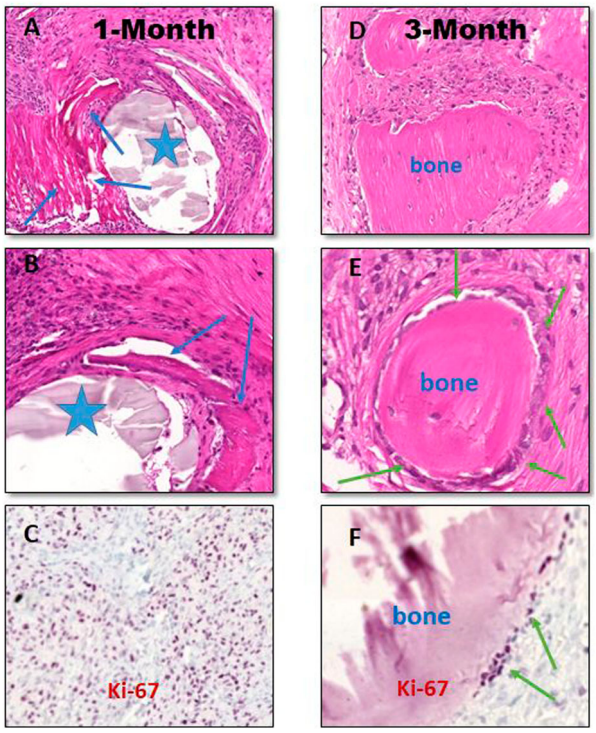

Figure 8. Histopathology of in vivo effects of β-tricalcium-phosphate-aerogel (β-TCP-AE) compound for scaffolding and in turn ossification to restore the 8 mm cylindrical bone defects in rat's calvarial skull bones 1 month (left panel) and 3 month after the surgical substitutionary interventions (right panel). Representative images are shown obtained from formalin-fixed paraffin-embedded decalcified tissue sections stained with hematoxylin-eosin (A–B and D–E), and immunohisto-chemistry for Ki-67 (C and F), respectively. Following one month of bone defect replaced with β-TCP-AE, there is a rapid injury- and foreign material-induced inflammation with granulation tissue formation that tends to fibrose and calcify with early ossification (A-B, blue arrows) around the exogenous compound (asterisks). C, Dense nuclear positivities (dark purple dots) among inflammatory and mesenchymal cells highlight leukocyte, fibroblasts and osteoblasts in active cell-cycle. D-E, Following a three-month duration of cylindrical bone defect replacement with β-TCP-AE, the hole became filled by islets of well-developed solid bone tissues embedded in moderately matured (less cellular) connective tissue with significantly decreased active inflammatory cells. F, However, based on Ki-67 immunohistochemistry, the bone-associated osteoblasts (green arrows) remain in active cell cycle (dark purple dots) indicating progressive ossification inside the defect. Original magnifications: A and D, *10x*; B, *20x*; E, *40x*; C and F, *20x*. For immunohistochemical images, a methyl-green nuclear counter-staining were used (C and F).

while most of the aerogel components became eliminated. Based on our combined results, this silica-based composite type, β-TCP-AE appears applicable as a novel scaffold ceramic in different areas of the dentistry, where a development of an anchoring new bone formation is a need.

Disclosure statement

No potential conflict of interest was reported by the authors.

Funding

This work was supported by European Social Fund: [Grant Number GINOP-2.3.2-15-2016-00011]; European Social Fund: [Grant Number GINOP-2.2.1-15-2017-00068]; European Social Fund: [Grant Number GINOP-2.3.2-15-2016-00041]; European Social Fund: [Grant Number GINOP-2.3.2-15-2016-00022].

ORCID

Farkas Kerényi http://orcid.org/0000-0003-3631-2770
István Lázár http://orcid.org/0000-0001-6006-7782

References

[1] Olszta MJ, Cheng X, Jee SS, et al. Bone structure and formation: a new perspective. Mater Sci Eng: R: Rep. 2007;58(3):77–116.
[2] Hench LL. The story of bioglass. J Mater Sci Mater Med. 2006;17(11):967–978.
[3] Schimming R, Schmelzeisen R. Tissue-engineered bone for maxillary sinus augmentation. J Oral Maxillofac Surg. 2004;62(6):724–729.
[4] Kistler SS. Coherent expanded aerogels and Jellies. Nature. 1931;127:741.
[5] Lázár I, Bereczki HF, Mano S, et al. Synthesis and study of new functionalized silica aerogel poly(methyl methacrylate) composites for biomedical use. Polym Compos. 2015;36(2):348–358.
[6] Lázár I., Fábián I. A continuous extraction and pump-less supercritical CO2 drying system for laboratory-scale aerogel production. Gels. 2016;2(4):26–40.
[7] Kuttor A, Melinda S, Rente T, et al. Preparation and application of highly porous aerogel-based bioactive materials in dentistry. Front Mater Sci. 2014;8 (1):46–52.
[8] Jokay I, Soós G, Répássy G, et al. Apoptosis in the human inner ear. Detection by in situ end-labeling of fragmented DNA and correlation with other markers. Hear Res. 1998;117(1–2):131–139.
[9] Tsakiris I, Torocsik D, Gyongyosi A, et al. Carboxypeptidase-M is regulated by lipids and CSFs in macrophages and dendritic cells and expressed selectively in tissue granulomas and foam cells. Lab Invest. 2012;92(3):345–361.
[10] Szabo K, Papp G, Dezso B, et al. The histopathology of labial salivary glands in primary Sjogren's syndrome: focusing on follicular helper T cells in the inflammatory infiltrates. Mediators Inflamm. 2014;2014:11. Article ID 631787. https://doi.org/10.1155/2014/631787.
[11] Dong M, Jiao G, Liu H, et al. Biological Silicon Stimulates collagen type 1 and Osteocalcin synthesis in human Osteoblast-like cells through the BMP-2/Smad/RUNX2 Signaling Pathway. Biol Trace Elem Res. 2016;173(2):306–315.
[12] Robaszkiewicz A, Erdelyi K, Kovacs K, et al. Hydrogen peroxide-induced poly(ADP-ribosyl)ation regulates osteogenic differentiation-associated cell death. Free Radic Biol Med. 2012;53(8):1552–1564.
[13] Gomes-Cornelio AL, Rodrigues EM, Mestieri LB, et al. Cytotoxicity and genotoxicity of calcium silicate-based cements on an osteoblast lineage. Braz Oral Res. 2016;30(1). pii: S1806-83242016000100247. doi:10.1590/1807-3107BOR-2016.vol30.0048.